

## RESEARCH ARTICLE

# Robust Design of Autofocused Airy Beam-Based Multifocal Metalens With Tunable Intensities

FATEMEH BAZOUBAND<sup>1</sup>, MAHDIEH HASHEMI<sup>1</sup>, ELAHEH BAZOUBAND<sup>1,2</sup>,  
RASHID A. GANEEV<sup>3,4,5,6</sup>, AND ANDRA NARESH KUMAR REDDY<sup>3</sup>

<sup>1</sup>Department of Physics, College of Science, Fasa University, Fasa 74617-81189, Iran

<sup>2</sup>Department of Physics, Shiraz University, Shiraz 71946-84334, Iran

<sup>3</sup>Laboratory of Nonlinear Optics, University of Latvia, 1004 Riga, Latvia

<sup>4</sup>Tashkent Institute of Irrigation and Agricultural Mechanization Engineers, National Research University, Tashkent 100000, Uzbekistan

<sup>5</sup>Department of Physics, Voronezh State University, 394006 Voronezh, Russia

<sup>6</sup>Department of Physics and Astronomy, Chirchik State Pedagogical University, Chirchik 111700, Uzbekistan

Corresponding author: Andra Naresh Kumar Reddy (naareddy@gmail.com; naresh.andra@lu.lv)

This work was supported in part by the European Regional Development Fund under Grant 1.1.1.5/19/A/003, and in part by the World Bank under Project REP-04032022-206.

**ABSTRACT** Optical metasurfaces with versatile focal properties have great importance and adaptability in photonic systems and potential applications. The unique capability of the ultra-compact device in forming and modulating light fields is triggered to configure multifocal setups. This study introduces a geometric metasurface consisting of dielectric cross-shaped metaatoms with a suitable phase profile operating in the visible regime that can transport the conjugate focal spot of the auto-focused Airy beam (AFAB) into real space by adding the proper convex lens profile and resulting in three foci whose positions and intensities can be adjusted without redesigning metaatoms architecture. The cross-shaped meta-atoms with complete control of the amplitude and phase of the incident light have considered diverse functionalities for the x- and y-components of the incident light, generating six focal spots with high adjustable intensities shown in free space. The proposed hybrid metalens has shown robustness against change in geometrical design while controlling multifocal setups, which can be useful in developing polarization-sensitive devices, photonics, medicine, micromachining and imaging applications to realize beneficial results.

**INDEX TERMS** Dielectric metasurfaces, Airy beams, metalens, diffraction, propagation.

## I. INTRODUCTION

Optical metasurfaces are adopted in developing beam conditioning technology, and devices have great importance due to their unique capability and characteristics [1]. Specifically, metasurfaces employed to generate autofocused Airy beams feature a long depth of focus that exhibits the anti-diffraction and self-healing properties during free-space propagation is potentially important in numerous applications [2], [3], [4], [5], [6]. From earlier results, it is concluded that two Airy beams that are mirror symmetric to each other relative to their launching plane can form autofocused non-diffracting Airy beam (AFAB), creating two conjugate focal spots, one is at the real focus, and the other

one is the virtual one [2], [3], [4], [5], [6], [7]. To verify the existence of a virtual image (spot), the convex lens phase profile was added to the AFA profile to bring the virtual focal spot into the real space, resulting in bifocal metalens and transforming into a multifocal lens [7], [8]. Recently, different metalenses have drawn attention due to their bifocal setups for the incident light under different polarization conditions. In this context, metalens was demonstrated to form two focal spots, one under x-polarization and the other under y-polarization of incident light [9]. A pancharatnam-berry phase was incorporated in the broadband achromatic metalens to converge the light, thereby creating focal points  $f_L$  and  $f_R$ , whose positions were controlled when the metalens was illuminated by left circularly polarized light (LCP) and right circularly polarized light (RCP), respectively [10], [11]. Bifocal metalens combined with liquid crystals was used

The associate editor coordinating the review of this manuscript and approving it for publication was Zhongyi Guo.

to achieve electrically tunable focusing and imaging at visible wavelengths [12]. Transmissive metalens with the required phase profile under the illumination of the incident light with orthogonal components was realized to form two independent focal spots [13]. Meanwhile, several multifocal metalenses with different functionalities were reported, such as high focusing efficiency [14], polarization detection of THz beams [15], polarization rotated focal points [16], longitudinal focusing with a tunable intensity ratio [17], helicity dependent multiple focal points [18] and longitudinal focusing with circular polarization [19], controlled multiphase imaging [20]. Besides, Airy beam patterns were produced using diffractive optical elements, which are widely useful components in applications [21], [22], [23]. However, the efficacy of metasurfaces in forming Airy and AFAB was proven to be more excellent than traditional diffractive optical elements and bulky structures while simultaneously modulating and controlling the phase and amplitude of incident light [24], [25]. Specifically, AFA beam-based metalens proposed to form a bifocal setup with high focusing efficiency and facilitates the flexible use of space while assigning focus spots [26]. Earlier, metalens developed to operate in the THz frequency range, comprised of splitting resonators (metaatoms) with different geometry and spins, were demonstrated to form a light focusing with a tunable number of focal points [27]. Besides, several nice works were reported on multifocal and multifunctional optical metasurfaces, such as multifunctional metalens whose focal line and point are interchangeable based on the incident light helicities [28], polarization-resolved multifocal metalens operates in the NIR range, perform polarization transformation and forms six-beams or focal spots from the incident LP light [29], a metalens designed to focus two wavelengths with inverse spin states, and it can focus four beams with different wavelengths and inverse spin states [30], a dielectric metalens operates in SWIR regime developed to focus along transverse and longitudinal directions for different spin states of the incident light [31] [Table 1].

In contrast to earlier investigations on AFA-based metalens designs with single focal and multifocal setups, the present paperwork focused on designing a unique multifocal focusing AFA metalens having the ability to generate six focal spots simultaneously so that the focal intensities can be tuned without repatterning the architecture of metaatoms. To achieve this special functionality, we have chosen silicon cross-shaped metaatoms with a specific geometry on the surface of a silica substrate. With the help of the proposed dielectric hybrid metalens design with a suitable phase profile, we not only gain access to the virtual space of the AFA beam but are also allowed to transfer the virtual focal spot into real space, thereby forming a bifocal setup. By considering the focal spot of the added convex lens, three longitudinal focal spots are also visible in free space. When the hybrid metalens subjects to 45° Linearly polarized light, each orthogonal component x and y produce three focal spots at desired positions in free space simultaneously, realizing

that intensities of focal spots as a function of the polarization angle of the incident light without changing the metalens pattern. Most significantly, reported AFAB-based multifocal metalens combining orthogonal components formed focal point arrangements that exhibit robust focusing effect has promising applications in biomedical imaging, photonics, particle manipulation, etc.

This paper is organized as follows: section II presents metalens geometry, unit cell specifications, and theoretical relations. In section III, we evaluate the performance of hybrid AFA metalens for incident light that is 45° Linearly polarized. Comparison with state-of-the-art methods discussed in section IV. In section V, we discussed the fabrication process of the proposed metalens. Finally, conclusions are discussed in section VI.

## II. METALENS DESIGN AND THEORY

In this section, we develop theoretical concepts of AFAB generation, convex metalenses, and their hybrid application to develop a metasurface with six focal spots simultaneously. An Airy beam through ignoring the decay factor evolves according to Eq. (1) [32],

$$\varphi(s, \xi) = Ai[s - 0.25\xi^2]e^{-i\frac{\xi^3}{12} + i\frac{s\xi}{2}}. \quad (1)$$

The AFAB is generated by the two-launching mirror-symmetric Airy beams as  $U(s, \xi) = \varphi(s, \xi) + \varphi(s', \xi)$  along the  $x$ -axis, where  $Ai[\dots]$  denotes the Airy function,  $s = (x - x_l)/x_0$ , and  $s' = -(x - x_l)/x_0$  are dimensionless transverse coordinates while  $x_0$  is an arbitrary transverse scaling factor and  $x$  is the geometric coordinate along the  $x$ -direction. Here  $x_l$  in  $s$  and  $s'$  terms represent the launching position of the two Airy beams, which guarantees the interference of the two generated Airy beams.  $\xi = z/kx_0^2$  is the normalized propagation distance, where  $z$  is the geometrical coordinate along the propagation direction and  $k = 2\pi/\lambda$  is the wavenumber of the incident light. Note that the generated real focal spot of AFAB occurs at the coincidence point of the two consisting Airy beams at  $z_{\max} = kx_0^2\sqrt{1 + x_l/x_0}$  in the real space with  $z > 0$  [7]. By changing  $z$  to  $-z$  in Eq. (1) and converting  $U(s, \xi)$  to  $U(s, -\xi)$ , the real-valued function of AFAB is obtained by  $U(s, \xi) + U^*(s, \xi)$ , and the virtual focal point on the opposite side of light propagation is produced by the second plane that wave wakes off the optic axis in the semi-space of  $z < 0$ . The virtual focus is not accessible in practice, and for transferring it into real space, adding a suitable convex lens phase profile can help. The common lens equation that expresses the quantitative relationship between the object distance (P), the image distance (Q), and the focal length (f) are stated as follows:

$$\frac{1}{P} + \frac{1}{Q} = \frac{1}{f}. \quad (2)$$

By adding the lens phase profile to the AFAB phase profile, the virtual focal point of AFAB as an imaginary object to the

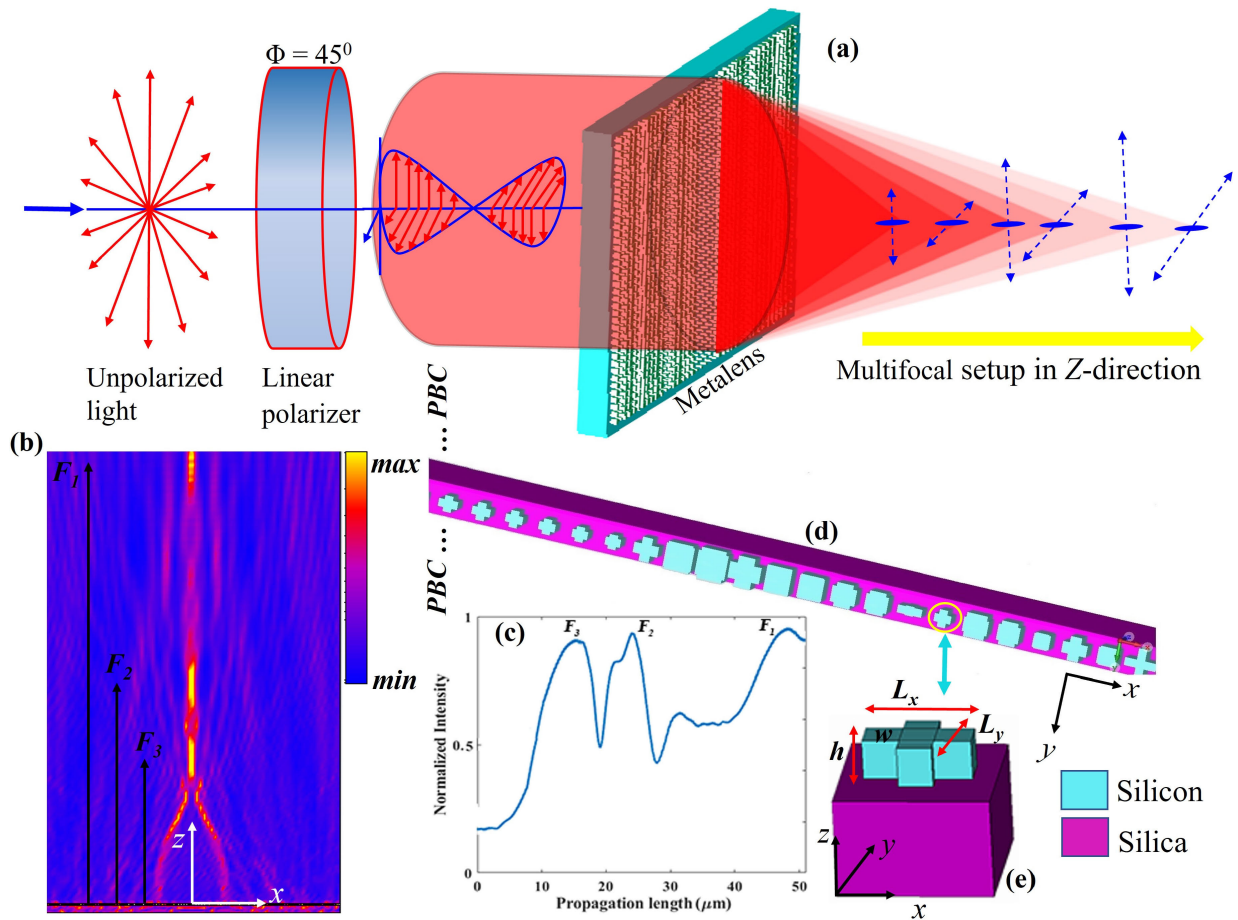


**FIGURE 1.** (a) Schematic illustration of the optical setup with the multifocal AFAB-based metalens transforms the incoming 45° linearly polarized light into a multifocal setup in the z-direction (free-space). (b) Representative intensity distribution of three focal points in the x-z plane. (c) One-dimensional intensity distribution for three-focal spots arrangement plotted as a function of propagation length ( $\mu\text{m}$ ) in the z-direction. (d) Surface 3D view of selected metaatoms and PBC in the y-direction. (e) Silicon cross-shaped metaatom unit cell on the Silica substrate having height  $h$ , width  $w$  and length along  $x$ - and  $y$ -direction are  $L_x$  and  $L_y$ .

lens can be transferred into the real space to increase the real focal spots number in the real space to two. The phase profile of a convex lens to focus the light at the focal length  $f$  is expressed as,

$$\phi(x, \lambda) = \frac{2\pi}{\lambda} \left( \sqrt{x^2 + f^2} - f \right). \quad (3)$$

By multiplying the phase profile of AFAB to Eq. (3), the dominant profile of the hybrid metasurface at  $z = 0$  will be obtained as,

$$U'(s, 0) = U(s, 0) \exp \left[ \frac{2\pi i}{\lambda} \left( \sqrt{x^2 + f^2} - f \right) \right]. \quad (4)$$

In this case, the arrangement of metaatoms along the x-axis will provide an AFAB with an extra real focusing spot. The spatial coordinate of the center of each metaatom along the x-direction is denoted by  $x$ .

Since the central amplitude of AFAB is zero [7], the focal spot of the lens that is multiplied to AFAB does not show itself. By partially modifying the amplitude and setting the

central part equal to 0.5, the focal spot of the lens is also presented, and the combination of AFAB and metalens leads to three real focal spots.

A schematic illustration of the optical setup with multifocal AFAB-based metalens is shown in **Figure 1(a)**. An unpolarized light from the laser source is converted into a linearly polarized light at 45° degrees after passing through a linear polarizer (angle of orientation,  $\Phi = 45^\circ$ ) and then radiated into the metalens. The resulting focal spots are formed at desired locations by the x- and y-components of incoming linearly polarized light. The metaatoms are arranged along the x-direction according to Eq. (4) and generate three focal spots, as shown in **Figure 1(b)**.

In **Figure 1(b)**, the first focal point ( $F_1$ ) is the real focus of AFAB that is generated at  $z = 49 \mu\text{m}$ , the convex metalens produces the second focal spot ( $F_2$ ) at  $z = 25 \mu\text{m}$ , and the third focal point ( $F_3$ ) is the real image of AFAB virtual focus at  $z = 18 \mu\text{m}$ . The one-dimensional intensity distribution for focal spots arrangement shown in **Figure 1(b)** is plotted as a function of propagation length in the

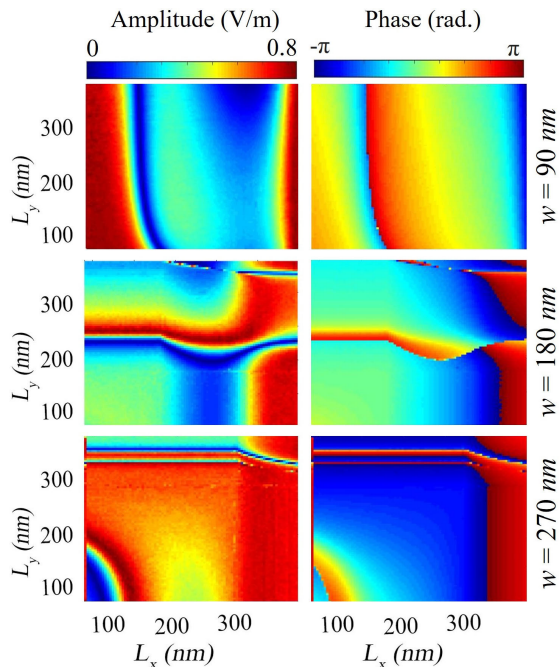


**FIGURE 2.** Amplitude and phase distributions of a transmitted electric field as a function of  $L_x$  and  $L_y$  for various values of  $w$ . Amplitude distributions shown in the first column are obtained when the incident light is x-polarized. Phase distributions shown in the second column are detected when the incident light is x-polarized [33].

z-direction. The resultant 1D-intensity distribution of the focal spots arrangement is illustrated in **Figure 1(c)**, and the intensity peaks corresponding to individual focal spots  $F_1$ ,  $F_2$ , and  $F_3$  are detected. In the present work, a linearly polarized light at the wavelength  $\lambda = 700$  nm illuminates the metaatoms structure grown on the Silica substrate, and the transmitted light propagates along the  $z$  direction in the free space. The periodic boundary condition (PBC) has been applied in the  $y$  direction, as shown in **Figure 1(d)**. The desired metaatoms considered in this study are the cross-shaped metaatoms whose unit cell structure is shown in **Figure 1(e)**, with the fixed height of  $h = 200$  nm and variable lengths along  $x$  and  $y$  directions range  $90$  nm  $< L_x < 350$  nm and  $100$  nm  $< L_y < 360$  nm. The structure of cross-shaped metaatoms is such that they can apply different functionalities to both  $x$ - and  $y$ -components of the incident light simultaneously and create different focusing areas for each component, that the focal spots of  $x$  and  $y$ -components are called  $f_x$  and  $f_y$ .

Simultaneous excitation of electric and magnetic dipoles in these cross-shaped metaatoms, separately for  $x$  and  $y$ -components of the electric field of the incident light, and therefore, the possibility of full control of the transmitted light phase and amplitude through them is shown in our previously published paper [33]. **Figure 2** shows the amplitude and phase distribution of the transmitted electric field as a function of the cross-shaped metaatoms geometrical parameters, lengths along  $x$ - and  $y$ -direction ( $L_x$ ,  $L_y$ ) and

width ( $w$ ). However, geometrical parameters height ( $h$ ) and nearest-neighbourhood distance ( $d$ ) hold fixed values. The range of geometrical parameters for the cross-shaped unit cells is considered as  $90$  nm  $< L_x < 350$  nm and  $100$  nm  $< L_y < 360$  nm in  $3$  nm steps, whereas the width ( $w$ ) values selected as  $90$ nm,  $180$ nm, and  $270$  nm. The distance between the center of two adjacent metaatoms is  $d = 360$  nm. The first column in **Figure 2** contains representative amplitude distributions of a transmitted  $x$ -polarized light field for various selected  $w$  values. The second column carries representative phase distributions of a transmitted  $x$ -polarized light field for various selected  $w$  values. For  $y$ -polarized incident light, amplitude and phase distributions are mirrored from one of the  $x$ -polarized amplitude and phase distributions with regard to the diagonal direction. For the given range of geometrical parameters, the selected  $w$  values make a full-phase and amplitude cover of both orthogonal components of the transmitted electric field. Besides, both transmitted  $x$ - and  $y$ -polarized electric fields gain maximum diffraction efficiency for the selected metaatoms.

It has worth of mentioning that, despite of previous studies that metalens was divided in some parts and each part was responsible for one focus [9], [17], in this paper, by using the special cross-shaped metaatoms that are able to fully control the  $x$ - and  $y$ -polarization simultaneously, the whole structure is responsible for all focal spots.

The possibility of defining different functionalities is considered for the  $x$ - and  $y$ -components of the incident light field. In this case, Eq. (4) should be written for both components by defining  $f$  as  $f_x$  and  $f_y$ . Satisfying these relations will make an AFAB-based metalens with six focal spots because each component can generate three focal spots. When the same functionality is considered for the  $x$ - and  $y$ -components of the incident light ( $f_x = f_y$ ), the AFAB-based metalens focuses the incident light at three focal spots, as shown in **Figure 1(b)**, where the incident light has  $45^\circ$  linear polarization.

### III. RESULTS AND DISCUSSIONS

The first step for designing the multifocal AFAB-based metalens to produce six focal spots simultaneously is delivering the required phase and amplitude profile with the metaatoms that are selected based on Eq. 4. The characteristics of the six desired focal spots of this study are as follows, the focal spot of AFAB for  $x$ -component of incident light is set to  $F_{1x} = 70\lambda$ . Therefore, its virtual focal spot is generated at  $z = -70\lambda$ . When we add the proper metalens profile and consider this virtual spot as an object of metalens ( $P = -70\lambda$ ), by considering the focal spot of the lens at  $f \equiv F_{2x} = |P/2| = 35\lambda$ , the real image of an object at  $P = -70\lambda$  is generated at  $Q(\equiv F_{3x}) = P/3 = 23.3\lambda$ , according to Eq. (2). Therefore, we expect three focal spots at  $F_{1x} = 70\lambda$ ,  $F_{2x} = 35\lambda$  and  $F_{3x} = 23.3\lambda$ . For  $y$ -polarization by the same formalism, the focal spots are set as  $F_{1y} = 50\lambda$ ,  $F_{2y} = (50/2)\lambda$  and  $F_{3y} = (50/3)\lambda$ .

The theoretical phase profile for combining the AFAB and the metalens to focus the  $x$ -component of incident light at the

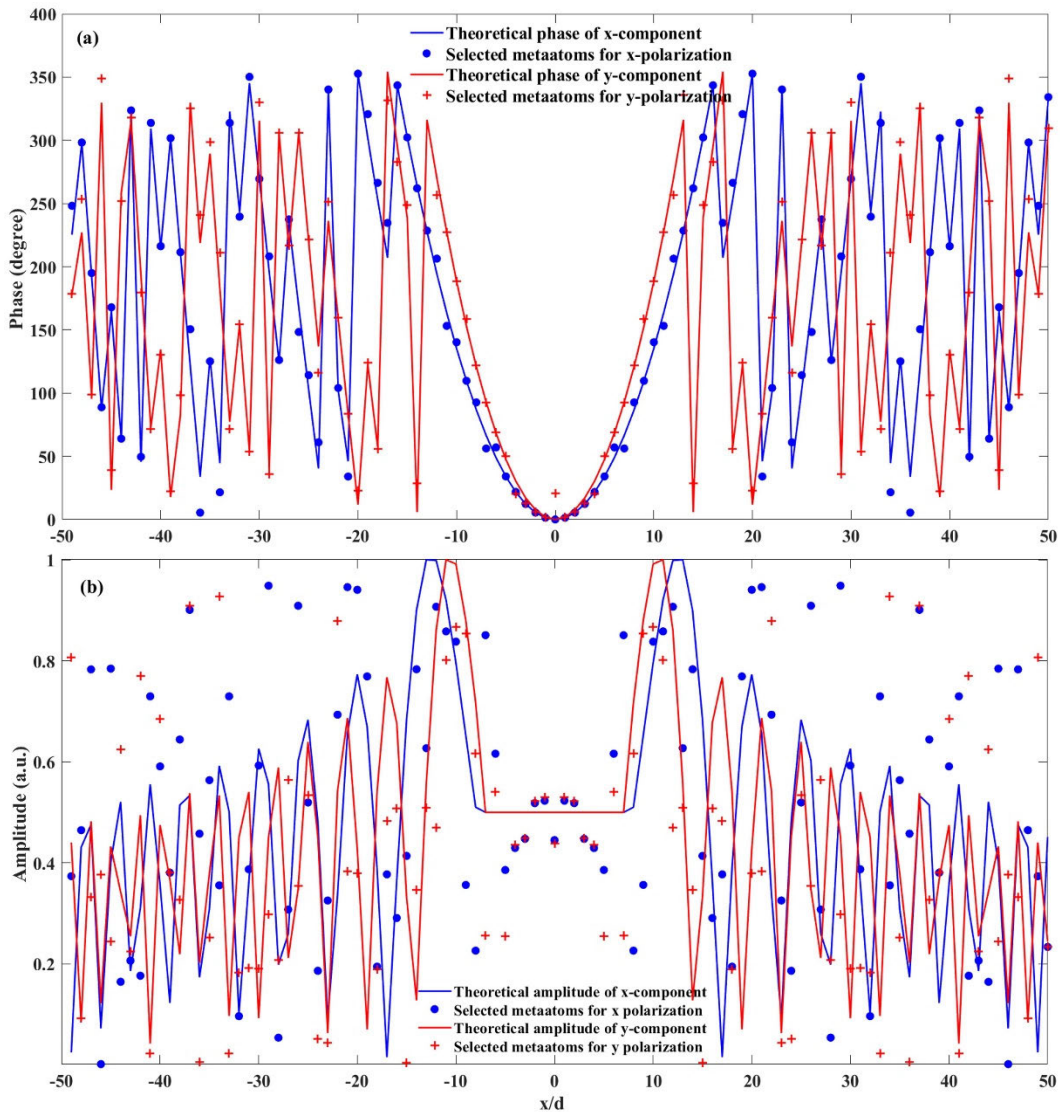


**FIGURE 3.** (a) The phase profile of AFAB combined with metalens for producing six focal spots, blue (red) lines, and marks are the theoretical phase and the phase of selected metaatoms for x-(y) polarization, respectively. (b) The amplitude of AFAB multiplied by metalens after modification to have nonzero amplitude at the center for producing six focal spots, blue (red) lines, and marks are the theoretical amplitude and the amplitude of selected metaatoms for x-(y) polarization, respectively.

three mentioned focal spots is shown by the solid blue curve in **Figure 3(a)**. Blue marks of **Figure 3(a)** show the phase of selected metaatoms that satisfy the required theoretical phase. Red-solid curves and red marks in **Figure 3(a)** show the theoretical phase and the phase of selected metaatoms for y- polarization, respectively. The required amplitude for generating the six focal spots and the amplitude of selected metaatoms to form the proposed multifocal structure is shown in **Figure 3(b)**. Blue (red)-solid curve and blue (red) marks show the required amplitude and the amplitude of selected metaatoms for x- and (y-) polarization, respectively. The nonzero value in the middle of the solid curves shows the amplitude modification for indicating the lens focusing, as discussed in the previous section. Since the

fulfilment of the required theoretical profiles should be satisfied for two components of x and y simultaneously, differences are seen in matching the theoretical amplitude or phase with that of selected metaatoms. For producing the AFAB-based metalens with six focal spots, the selected metaatoms of **Figure 3** are arranged along the x-direction by PBC in the y-direction. The one hundred metaatoms are considered for designing the metalens, and they are selected among 23000 metaatoms that are swept over the geometric parameters of metaatoms to full phase cover of  $0$  to  $2\pi$  [33].

The selected silicon cross-shaped metaatoms used in the current study substantially enhance the lens functionality. For the metalens design that consists of silicon cross-shaped metaatoms covered on the silica substrate, we used silicon

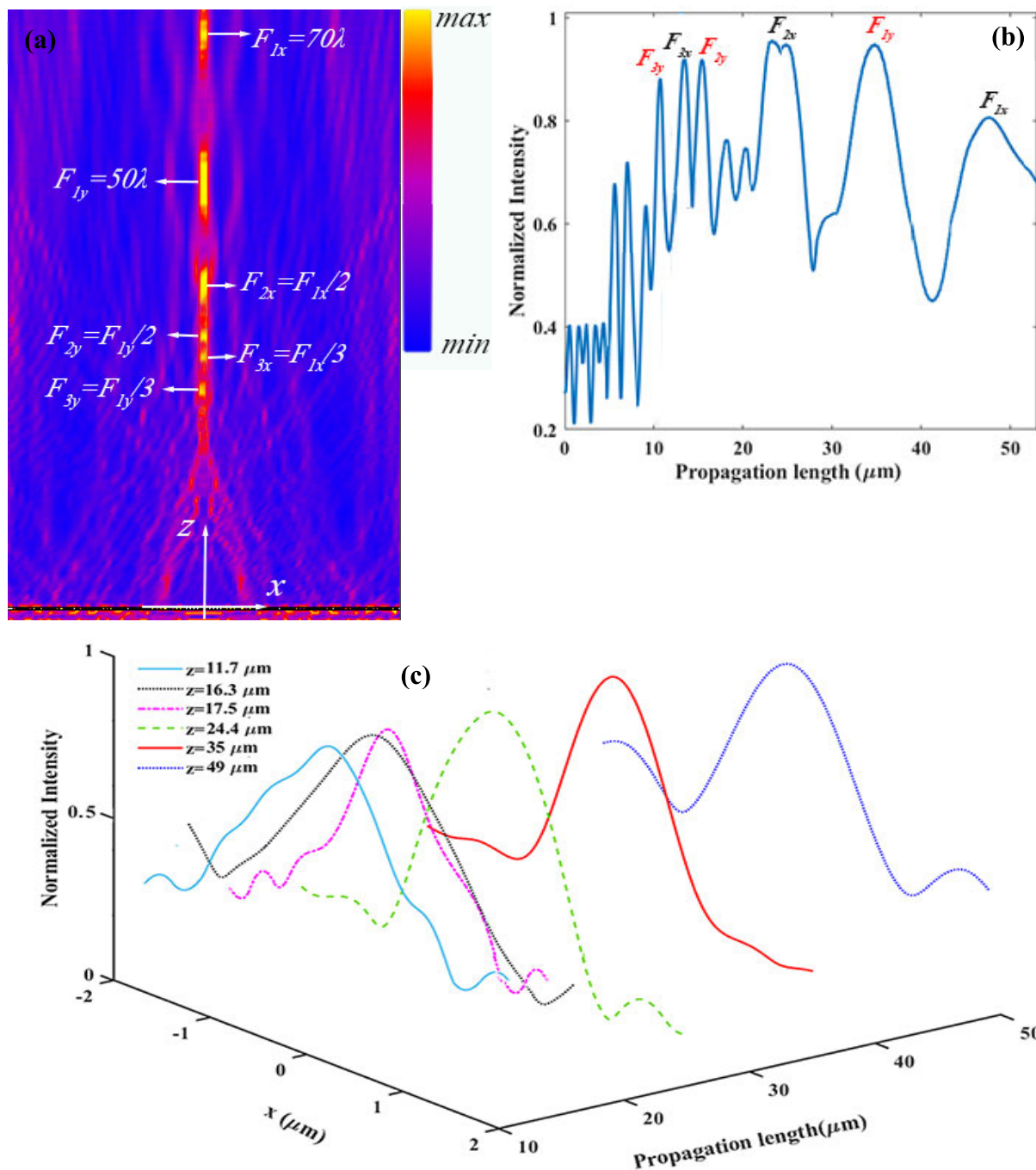


**FIGURE 4.** (a) The field distribution of AFAB combined with metalens for producing six focal spots at distances  $z = 49, 35, 24.4, 17.5, 16.3,$  and  $11.7 \mu\text{m}$  under the illumination of  $45^\circ$  Linearly polarized light. (b) One-dimensional intensity distribution for six-focal spots arrangement plotted as a function of propagation length ( $\mu\text{m}$ ) in the z-direction. (c) Cross-sectional intensity profiles of focal spots formed at different z distances.

(Si) with a high relative permittivity of 13.5 and silica ( $\text{SiO}_2$ ) with a permittivity of 2.1 and refractive indices of silica and silicon are chosen from [34]. Note that the transmission efficiency of employed cross-shaped metaatoms is about

80%. For better understanding, amplitude distributions of transmitted light fields as a function of the cross-shaped metaatoms geometrical parameters ( $L_x, L_y$  and  $w$ ) are evaluated, as shown in Figure 2. The focusing efficiency

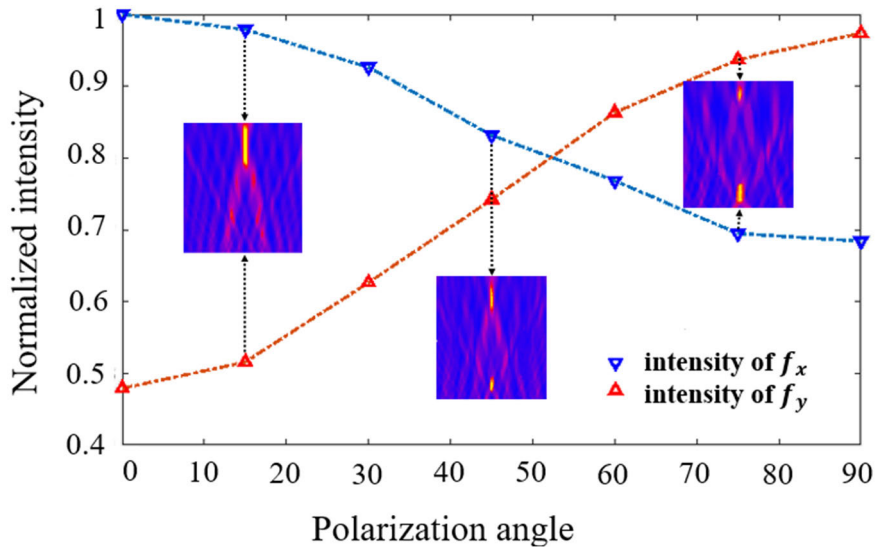


**FIGURE 5.** The normalized intensity of two focal spots of AFAB versus the polarization angles of LP incident light. The insets are the field distributions in the x-z plane for various polarization angles 15°, 45° and 75°.

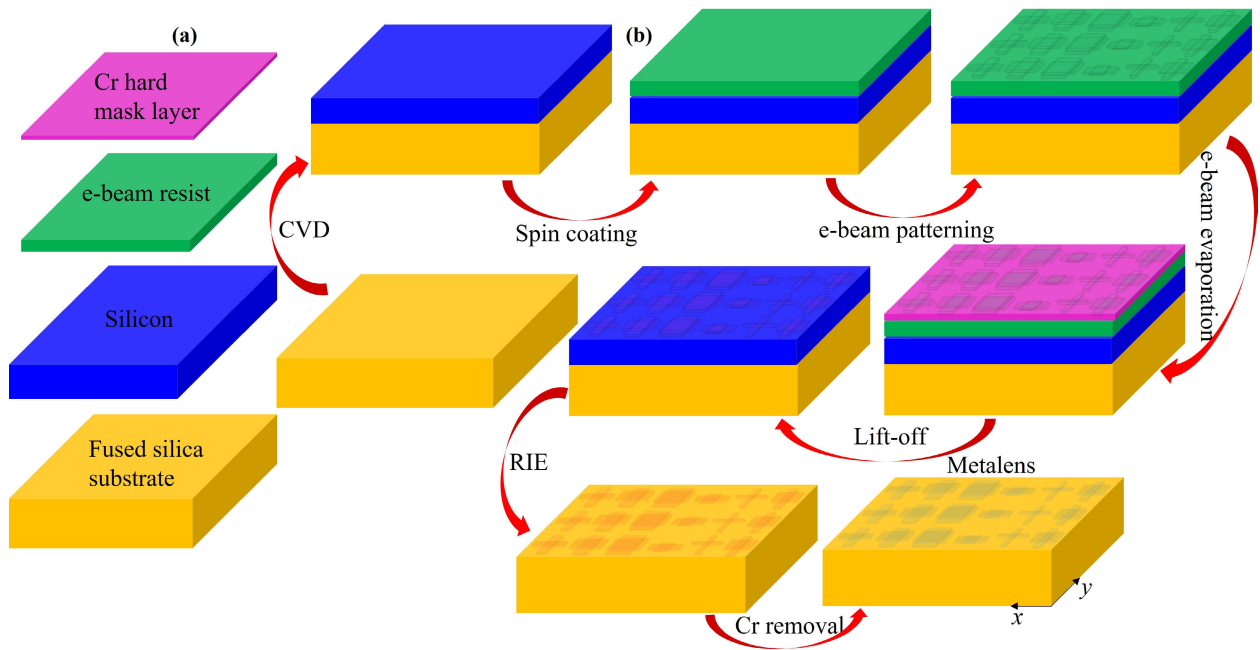


**FIGURE 6.** Materials and the process involved in the fabrication of dielectric multifocal metalens. (a) Arrangement of materials in the form of layers (b) Steps involved in synthesizing dielectric optical metasurface demonstrated as multifocal focusing metalens.

of the metalens can be defined as the ratio of accumulated energy around the focus to the total incoming energy. However, the proposed metalens is the multifocal focusing lens that rips the incident energy to each focal spot among six focal spots leading to low focusing efficiency.

The phase distributions of the transmitted electric field formed by the selected metaatoms sweep over the particular combinations of geometrical parameters  $L_x$ ,  $L_y$ , and  $w$  are already presented in **Figure 2**. The electric field distribution

of transmitted light in the x-z plane is shown in **Figure 4(a)**. The incident light has the 45° Linear polarization (LP) that each orthogonal component of x and y produces three focal spots at desired locations. However, as discussed in the next paragraph, the same metalens structure under LP light illumination has the benefit of adjustability by polarization angles. It is expected that when the distance between foci is controlled, performing complex additions or superposition of interference between foci is possible,

resulting in a needle-shaped beam that is escorted by a certain depth of focus. Note that extended focus imaging in free-space carries certain defects, which is an apparent effect. Maintaining a good focusing effect is tedious with the growing number of focal spots for the multifocal metalens. In the present study, the metalens region and phase distributions were carefully selected to prevent strong coupling effects between neighbouring focal spots, as shown in **Figure 4(a)**. However, the resultant field distribution shown in **Figure 4(a)** states that the different sections of the multifocal metalens, such as the convex lens profile and Autofocusing Airy beam profile, are individually responsible for the formation of six focal spots with an inhomogeneous length. The one-dimensional intensity distribution for the six-focal spots arrangement shown in **Figure 4(a)** is plotted as a function of propagation length in the z-direction. The resultant 1D-intensity distribution of the six-focal spots arrangement is illustrated in **Figure 4(b)**, and the intensity peaks corresponding to individual focal spots ( $F_{1x}$ ,  $F_{1y}$ ,  $F_{2x}$ ,  $F_{2y}$ ,  $F_{3x}$ , and  $F_{3y}$ ) are detected. However, undesirable ripples were spotted between peaks that do not influence the focal range and the distribution of the multifocal spot arrangement formed by the dielectric metalens. Besides, cross-sectional intensity profiles of individual focal spots are plotted as a function of propagation length ( $\mu\text{m}$ ), as illustrated in **Figure 4(c)**.

The significance of dielectric metalens structure when illuminated by LP light is that we can arbitrarily change the intensity of focal spots by varying the angle of polarization without changing the geometrical configuration of AFAB-based metalens, which is time-saving and efficient in practical applications. To avoid the complexity of having six focal spots and a better understanding of this salient feature, we design an AFAB metalens without the inclusion of a convex lens profile that focuses the x- and y-components at  $f_x = 70\lambda$  and  $f_y = 50\lambda$  in **Figure 5**. We calculated the relationship between the normalized intensity of two focal spots and the polarization angles (PA) of the incident light (as shown in **Figure 5**). The Blue and Red marks are the normalized intensity of focal spots produced by the x- and y-component of the incident light, respectively, under the illumination of LP light with different polarization angles. The results show that the intensity of two foci could be flexibly adapted by changing the PA of the incident beam without repatterning the metaatoms. The insets of **Figure 5** show the transmitted electric field distribution in the x-z plane for the PA  $15^\circ$ ,  $45^\circ$  and  $75^\circ$ . Under the illumination of  $15^\circ$  polarized light, which is very close to x-polarization, the intensity of the focal spot of the x-component that appears at  $f_x = 70\lambda$  is strong. By increasing the PA to  $45^\circ$ , the focal spot of the y-component found at  $f_y = 50\lambda$  also stands out, and it will be stronger under the illumination of light with PA =  $75^\circ$ . Therefore, by designing the unique metasurface, we can have multifocal spots whose intensity can be tunable by varying the polarization angle of the incident light, which is valuable in generating focal spots with controlled power

densities useful in numerous applications, such as material processing, micromachining, optical trapping, and medical treatments.

#### IV. COMPARISON WITH STATE-OF-THE-ART METHODS

The present investigation selected the transmission mode optical metasurface structure built by cross-shaped silicon metaatoms to demonstrate their adequacy and flexibility in amplitude, and phase sweep is vital for generating non-diffracting autofocused Airy beam (AFAB) distribution with a multi-focusing effect. However, to attain the phase and amplitude of transmitted light through selected metaatoms, the PBC was placed in the y-direction. Further, the phase and amplitude profiles of AFAB combined with metalens apply different functionalities for the x- and y-components of the incident field simultaneously, leading to form the required light field distributions that have proven to be a flexible design of multifocal metalens can generate the series of six focal spots in space, is a significant advancement that we touched in this work. To quantitatively compare the multifocal metalens setups investigated in various research works relative to the present work, we listed several parameters in **Table 1** to compare operational conditions, chemical composition and the outcome of various multifocal setups illuminated by the light field with the selected polarization state.

#### V. ANTICIPATED MANUFACTURING PROCESS OF DIELECTRIC MULTIFOCAL METALENS

The proposed dielectric optical metasurface consists of cross-shaped nano-unit cells (fundamental building blocks) that can control and manipulate the phase and amplitude of transmitting light. Dielectric metalenses don't suffer from restrictions such as the confined possibility of guiding the phase and absorption losses when the light passes through the optical metasurface. Typically, dielectric metalenses show exceptional performance than other alternatives and traditional optical components. However, the fabrication of such optical metasurfaces with multifocal functionality is a challenging task to complete.

**Figure 6(a)** describes materials and layers used to fabricate multifocal metalens. **Figure 6(b)** reveals various steps to develop the proposed dielectric multifocal metalens. First, an intrinsic polycrystalline silicon layer of an optimized thickness (200 nm) will be grown on the transparent fused silica substrate using low-pressure chemical vapour deposition (CVD) at the predefined and controlled temperature. The dielectric layer can be patterned with fundamental building blocks and transformed into multifocal metalens with electron-beam lithography (EBL) with subsequent lift-off technology and the selected reactive ion etching (RIE) process. With spin coating, the e-beam resist can be deposited on the dielectric layer (Si), and the EBL with a lift-off process can be applied to create the proposed cross-shaped patterns with the chromium (Cr) hard-mask layer. Later, the inductive coupled plasma-based RIE can be used to etch the silicon

**TABLE 1.** Comparative study of geometrical configuration and performance associated with various multifocal metalens setups.

| Ref. Num. | Input field polarization | Operating wavelength $\lambda(\mu m)$ | Focal length          | Metaatom composition | Lens thickness ( $\mu m$ ) | Outcome  |
|-----------|--------------------------|---------------------------------------|-----------------------|----------------------|----------------------------|--|
| [7]       | Linear                   | 0.7                                   | 16, 25, 50 $\mu m$    | Silicon              | 0.2                        | Three focal spots were generated simultaneously by the whole metalens in the longitudinal direction                  |
| [9]       | Linear                   | 3000                                  | $\sim 3, 5 \lambda$   | Copper               | 100                        | Two focal spots were generated separately, each by the part of metalens in the longitudinal direction                |
| [10]      | Linear                   | 0.532                                 | $\sim 10, 13 \mu m$   | TiO <sub>2</sub>     | 0.6                        | Two focal spots were generated simultaneously by the whole metalens in the longitudinal direction                    |
| [11]      | Circular                 | 0.5- 0.7                              | $\sim 0.4, 0.5 \mu m$ | TiO <sub>2</sub>     | 0.8                        | Two focal spots were generated separately by the whole metalens in the longitudinal direction                        |
| [12]      | Circular                 | 0.633                                 | $\sim 4, 7 mm$        | Silicon              | 0.5                        | Two focal spots were generated separately by the whole metalens in the longitudinal direction                        |
| [13]      | Circular                 | 0.532                                 | 40 $\mu m$            | TiO <sub>2</sub>     | 0.6                        | Two focal spots were generated simultaneously by the whole metalens in the transverse plane                          |
| [14]      | Circular                 | 0.532                                 | 5, 12 $\mu m$         | Silver               | 0.1                        | Two focal spots were generated separately, each by the part of metalens in the longitudinal and transverse direction |
| [15]      | Circular                 | 261                                   | 5 mm                  | Gold                 | 0.15                       | Four focal spots were generated simultaneously by the whole metalens in the transverse plane                         |
| [16]      | Linear                   | THz wave                              | 5 mm                  | Silicon              | 500                        | Two focal spots were generated separately by the whole metalens in the transverse plane                              |
| [17]      | Linear, Circular         | 0.8                                   | 2, 4 $\mu m$          | Gold nano hill       | 0.03                       | Two focal spots were generated simultaneously, each by the part of metalens in the longitudinal direction            |
| [18]      | Circular                 | 500                                   | 4 mm                  | Silicon              | 500                        | Two focal spots were generated simultaneously by the whole metalens in the transverse plane                          |
| [33]      | Linear                   | 0.7                                   | 7, 10.5 $\mu m$       | Silicon              | 0.2                        | Two focal spots were generated simultaneously by the whole metalens in the longitudinal direction                    |
| [26]      | Linear                   | 0.7                                   | 30, 60 $\mu m$        | Silicon              | 0.2                        | Two focal spots were generated simultaneously by the whole metalens in the longitudinal direction                    |
| [27]      | Linear                   | 0.476                                 | 3, 9 $\mu m$          | Aluminum             | 5                          | Two focal spots were generated simultaneously by the whole metalens in the longitudinal direction                    |
| [28]      | Circular                 | 0.640                                 | 0.198 $\mu m$         | Gold                 | 0.04                       | Dual-polarity lenses generated to focal spots separately by the whole metalens                                       |
| [29]      | Linear                   | 0.850                                 | 90 $\mu m$            | Silicon              | 0.5                        | Six focal spots were generated simultaneously, each by the part of metalens in the transverse plane                  |
| [30]      | Linear                   | 0.765, 1.3                            | 4 $\mu m$             | Gold nano hill       | 0.1                        | Two focal spots were generated simultaneously by the whole metalens in the transverse plane                          |
| [31]      | Linear                   | 1.5                                   | 4, 8 $\mu m$          | Silicon              | 0.8                        | Two focal spots were generated simultaneously by the whole metalens in the longitudinal and transverse direction     |

layer (poly-Si) along the patterned chromium (Cr) layer. Further, chromium masks can be removed using etchants such as mixtures of perchloric acid and ceric ammonium nitrate, resulting in metalens with multifocal functionality. The resultant metalens consists of 100 cross-shaped metaatoms with a periodicity of  $0.36 \mu\text{m}$ , and the total length or diameter of the metalens ( $D$ ) equals  $36 \mu\text{m}$ . **Figure 6(b)** illustrates the geometrical arrangement of metaatoms that can be grown on the surface of the substrate and replicates the geometry of metaatoms and their PBC (set in the  $y$ -direction), as shown in **Figure 1(d)**. The scanning electron microscope (SEM) can reveal the details of the geometrical configuration, dimensions, and period of metasurface building blocks. Finally, the performance of the metalens mounted on the high-precision stage will be experimentally investigated with the optical scheme, as shown in **Figure 1(a)**. It is advised to use an autocollimator to align the incident  $45^\circ$  linearly polarized light to the centre of the metalens, and a beam expander with a spatial filtering unit adjusts the beam size, together can reduce operational defects.

## VI. CONCLUSION

The work proposed and demonstrated multifocal AFAB metalens to form six focal spots in space whose intensities are tunable. By modulating the phase profile of AFAB metalens into a suitable form, the virtual focal spot of AFAB is transformed into real space. Besides, the focal spot of the lens is presented, and thus three longitudinal focal spots have appeared in space. To accomplish all these functionalities, we adopt the silicon cross-shaped metaatoms employed in building the multifocal focusing metalens with the unique ability to use both  $x$ - and  $y$ -components of incident light with different functionality and focus each component in different locations simultaneously. Therefore, when the AFAB metalens is illuminated by linearly polarized light, each orthogonal component of incident light produces three focal spots. As a result, six focal spots are generated at desired locations in space by utilizing the full energy of the incident light. The important property of the generated focal spots is that their intensities are tunable as a function of the polarization angle of the linearly polarized incident light, and it is achieved without reconfiguring the metalens design, which is time and energy saving. It is beneficial in potential applications, such as micromachining, optical trapping, particle manipulation, optical imaging and laser material processing.

## REFERENCES

- [1] M. K. Chen, Y. Wu, L. Feng, Q. Fan, M. Lu, T. Xu, and D. P. Tsai, "Principles, functions, and applications of optical meta-lens," *Adv. Opt. Mater.*, vol. 9, no. 4, Feb. 2021, Art. no. 2001414.
- [2] I. Chremmos, P. Zhang, J. Prakash, N. K. Efremidis, D. N. Christodoulides, and Z. Chen, "Fourier-space generation of abruptly autofocusing beams and optical bottle beams," *Opt. Lett.*, vol. 36, pp. 3675–3677, Sep. 2011.
- [3] D. G. Papazoglou, N. K. Efremidis, D. N. Christodoulides, and S. Tzortzakis, "Observation of abruptly autofocusing waves," *Opt. Lett.*, vol. 36, pp. 1842–1844, May 2011.
- [4] Q. Fan, D. Wang, P. Huo, Z. Zhang, and T. Xu, "Autofocusing Airy beams generated by all-dielectric metasurface for visible light," *Opt. Exp.*, vol. 25, no. 8, pp. 9285–9294, Apr. 2017.
- [5] G. A. Siviloglou and D. N. Christodoulides, "Accelerating finite energy Airy beams," *Opt. Lett.*, vol. 32, no. 8, pp. 979–981, Apr. 2007.
- [6] J. Broky, G. A. Siviloglou, A. Dogariu, and D. N. Christodoulides, "Self-healing properties of optical Airy beams," *Opt. Exp.*, vol. 16, no. 17, pp. 12880–12891, Aug. 2008.
- [7] M. Hashemi, M. M. Shanei, and C. J. Zapata-Rodríguez, "Flexible design of multifocal metalenses based on autofocused Airy beams," *J. Opt. Soc. Amer. B, Opt. Phys.*, vol. 35, pp. 2864–2868, Nov. 2018.
- [8] D. G. Papazoglou, V. Y. Fedorov, and S. Tzortzakis, "Janus waves," *Opt. Lett.*, vol. 41, pp. 4656–4659, Oct. 2016.
- [9] H. Markovich, D. Filonov, I. Shishkin, and P. Ginzburg, "Bifocal Fresnel lens based on the polarization-sensitive metasurface," *IEEE Trans. Antennas Propag.*, vol. 66, no. 5, pp. 2650–2654, May 2018.
- [10] S. Tian, H. Guo, J. Hu, and S. Zhuang, "Dielectric longitudinal bifocal metalens with adjustable intensity and high focusing efficiency," *Opt. Exp.*, vol. 27, no. 2, pp. 680–688, 2019.
- [11] Z. Qian, S. Tian, W. Zhou, J. Wang, and H. Guo, "Broadband achromatic longitudinal bifocal metalens in the visible range based on a single nanofin unit cell," *Opt. Exp.*, vol. 30, pp. 11203–11216, May 2022.
- [12] T. Badloe, I. Kim, Y. Kim, J. Kim, and J. Rho, "Electrically tunable bifocal metalens with diffraction-limited focusing and imaging at visible wavelengths," *Adv. Sci.*, vol. 8, no. 21, Nov. 2021, Art. no. 2102646.
- [13] Y. Gu, R. Hao, and E.-P. Li, "Independent bifocal metalens design based on deep learning algebra," *IEEE Photon. Technol. Lett.*, vol. 33, no. 8, pp. 403–406, Apr. 15, 2021.
- [14] H. Lv, X. Lu, Y. Han, Z. Mou, and S. Teng, "Multifocal metalens with a controllable intensity ratio," *Opt. Lett.*, vol. 44, pp. 2518–2521, May 2019.
- [15] R. Wang, J. Han, J. Liu, H. Tian, W. Sun, L. Li, and X. Chen, "Multi-foci metalens for terahertz polarization detection," *Opt. Lett.*, vol. 45, pp. 3506–3509, Jul. 2020.
- [16] X. Zang, H. Ding, Y. Intaravanne, L. Chen, Y. Peng, J. Xie, Q. Ke, A. V. Balakin, A. P. Shkurinov, X. Chen, Y. Zhu, and S. Zhuang, "A multi-foci metalens with polarization-rotated focal points," *Laser Photon. Rev.*, vol. 13, Dec. 2019, Art. no. 1900182.
- [17] W. Wang, "Polarization-independent longitudinal multi-focusing metalens," *Opt. Exp.*, vol. 23, no. 23, pp. 29855–29866, 2015.
- [18] B. Yao, X. Zang, Y. Zhu, D. Yu, J. Xie, L. Chen, S. Han, Y. Zhu, and S. Zhuang, "Spin-decoupled metalens with intensity-tunable multiple focal points," *Photon. Res.*, vol. 9, no. 6, pp. 1019–1032, Jun. 2021.
- [19] X. Chen, M. Chen, M. Q. Mehmood, D. Wen, F. Yue, C.-W. Qiu, and S. Zhang, "Longitudinal multifoci metalens for circularly polarized light," *Adv. Opt. Mater.*, vol. 3, no. 9, pp. 1201–1206, Sep. 2015.
- [20] Z. Yao and Y. Chen, "Focusing and imaging of a polarization-controlled bifocal metalens," *Opt. Exp.*, vol. 29, pp. 3904–3914, Feb. 2021.
- [21] B. Yalozay, B. Soylu, and S. Akturk, "Optical element for generation of accelerating Airy beams," *J. Opt. Soc. Amer. A, Opt. Image Sci.*, vol. 27, no. 10, pp. 2344–2346, Oct. 2010.
- [22] C. Liu, L. Niu, K. Wang, and J. Liu, "3D-printed diffractive elements induced accelerating terahertz Airy beam," *Opt. Exp.*, vol. 24, no. 25, pp. 29342–29348, 2016.
- [23] A. Benstiti, K. Ferria, and A. Bencheikh, "Generation of a variety of Airy beams using a dynamic diffractive optical phase element," *J. Opt. Soc. Amer. B, Opt. Phys.*, vol. 37, no. 11, p. A45, 2020.
- [24] E.-Y. Song, G.-Y. Lee, H. Park, K. Lee, J. Kim, J. Hong, H. Kim, and B. Lee, "Compact generation of Airy beams with C-aperture metasurface," *Adv. Opt. Mater.*, vol. 5, no. 10, May 2017, Art. no. 1601028.
- [25] Z. Li, H. Cheng, Z. Liu, S. Chen, and J. Tian, "Plasmonic Airy beam generation by both phase and amplitude modulation with metasurfaces," *Adv. Opt. Mater.*, vol. 4, no. 8, pp. 1230–1235, Aug. 2016.
- [26] M. M. Shanei, M. Hashemi, and C. J. Zapata-Rodríguez, "Unconventional, efficient and flexible bifocal lens design by metalens and AFA beam combination," *J. Opt.*, vol. 21, no. 5, May 2019, Art. no. 055101.
- [27] M. Hashemi, A. Moazami, M. Naserpour, and C. J. Zapata-Rodríguez, "A broadband multifocal metalens in the terahertz frequency range," *Opt. Commun.*, vol. 370, pp. 306–310, Jul. 2016.
- [28] D. Wen, F. Yue, M. Ardrón, and X. Chen, "Multifunctional metasurface lens for imaging and Fourier transform," *Sci. Rep.*, vol. 6, no. 1, p. 27628, Jun. 2016.

- [29] F. Ding, B. Chang, Q. Wei, L. Huang, X. Guan, and S. I. Bozhevolnyi, "Versatile polarization generation and manipulation using dielectric metasurfaces," *Laser Photon. Rev.*, vol. 14, no. 11, Nov. 2020, Art. no. 2000116.
- [30] W. Wang, Z. Zhao, C. Guo, K. Guo, and Z. Guo, "Spin-selected dual-wavelength plasmonic metalenses," *Nanomaterials*, vol. 9, no. 5, p. 761, May 2019.
- [31] W. Wang, C. Kang, X. Liu, and S. Qu, "Spin-selected and spin-independent dielectric metalenses," *J. Opt.*, vol. 20, no. 9, Sep. 2018, Art. no. 095102.
- [32] M. A. Bandres, I. Kaminer, M. Mills, B. M. Rodríguez-Lara, E. Greenfield, M. Segev, and D. N. Christodoulides, "Accelerating optical beams," *Opt. Photon. News*, vol. 24, no. 6, pp. 30–37, 2013.
- [33] F. Bazouband, E. Bazouband, T. Golestanizade, A. J. Sadooni, M. Mousavifard, A. S. Karimullah, A. N. Kumar Reddy, and M. Hashemi, "Efficient arbitrary polarized light focusing by silicon cross-shaped metaatoms," *J. Phys. D, Appl. Phys.*, vol. 55, no. 9, Mar. 2022, Art. no. 095108.
- [34] E. Palik, *Handbook of Optical Constants of Solids* (Academic Press Handbook Series), vol. 2. New York, NY, USA: Academic, 1991.



**ELAHEH BAZOUBAND** received the M.Sc. degree from the Department of Physics, Institute for Advanced Studies in Basic Sciences. Currently, she is pursuing the Ph.D. degree with the Department of Physics, Shiraz University, Iran. She actively collaborates with researchers from the Department of Physics, College of Science, Fasa University, Iran. Her current research interests include metasurfaces and photonics.



**RASHID A. GANEEV** received the Ph.D. degree in physics from the Institute of Electronics, Tashkent, Uzbekistan, in 1987. He is currently an ERA Chair of quantum optics and photonics and the Head of the Laboratory of Nonlinear Optics, University of Latvia. He is the author of ten monographs based on his studies of the low- and high-order nonlinear optical properties of various materials. He has published more than 450 articles in peer-reviewed journals. His main research interests include light–plasma interactions, optical materials, nonlinear optics, photonics, nanomaterials, high-order harmonics generation, and laser physics.



**ANDRA NARESH KUMAR REDDY** received the M.Sc. degree in physics (electronics and instrumentation) from the Department of Physics, Osmania University, Hyderabad, Telangana, India, the M.Phil. degree in optics and thin-film technology from Bharathidasan University, India, and the Ph.D. degree from Osmania University, Hyderabad, in 2014. He held a Postdoctoral Researcher position in the Middle East and European countries from 2018 to 2022. He held a senior scientist position with Samara National Research University, Russia, from 2016 to 2018. He was an Assistant Professor of physics with various engineering colleges in Hyderabad, from 2013 to 2016. He is currently a Senior Researcher with the NSP FOTONIKA-LV and the University of Latvia, Riga, Latvia. His current research interests include diffractive optics, coupled lasers, structured light, beam shaping, optical imaging, PSF engineering, incoherent imaging, free-space optics, orbital angular momentum, nonlinear optics, nonlinear materials, meta-fibers, metalenses, optical metasurfaces, laser material processing, 3D-printed meta-fiber tips, and micro/nanofabrication.



**FATEMEH BAZOUBAND** received the M.Sc. degree in physics from the Vali-e-Asr University of Rafsanjan, Iran, and the Ph.D. degree from the Amirkabir University of Technology, Iran, in 2013. Currently, she is an Assistant Professor of physics with the College of Science, Fasa University, Iran. Her current research interests include free-electron lasers, photonics, metasurfaces, accelerators, and metalenses.



**MAHDIEH HASHEMI** received the M.Sc. degree in photonics from Shahid Beheshti University, Iran, and the Ph.D. degree from Shiraz University, Iran, in 2013. She was a visiting Research Scholar with the Technical University of Denmark. She was a Guest Researcher with the University of Valencia for a few months. Currently, she is an Associate Professor of physics with the College of Science, Fasa University, Iran. Her current research interests include plasmonics, metasurfaces, graphenes, and TMDCs.

...